Magnetic fields of Ap stars as a result of an instability

R. Arlt⋆ and **G. Rüdiger**

Astrophysikalisches Institut Potsdam, An der Sternwarte 16, D-14482 Potsdam, Germany

Received 30 May 2005, accepted 11 Nov 2005
Published online later

Key words Stars: chemically peculiar, magnetic fields – instabilities

Ap star magnetism is often attributed to fossil magnetic fields which have not changed much since the pre-main-sequence epoch of the stars. Stable magnetic field configurations are known which could persist probably for the entire main-sequence life of the star, but they may not show the complexity and diversity exhibited by the Ap stars observed. We suggest that the Ap star magnetism is not a result of stable configurations, but is the result of an instability based on strong toroidal magnetic fields buried in the stars. The highly nonaxisymmetric remainders of the instability are reminiscent of the diversity of fields seen on Ap stars. The strengths of these remnant magnetic fields is actually between a few per cent up to considerable fractions of the internal toroidal field; this means field strengths of the order of kGauss being compatible with what is observed. The magnetic fields emerge at the surface rather quickly; rough estimates deliver time-scales of the order of a few years. Since rotation stabilizes the instability, normal A stars may still host considerable, invisible toroidal magnetic fields.

1 Introduction

Chemically peculiar stars of types late B, A and early F are often accompanied by magnetic fields. We will call them Ap stars here collectively and will deal with the possible origin of the magnetic fields observed at the surfaces of these stars.

The observations of magnetic Ap stars show a large diversity of field strengths, topologies, and rotational periods. Only a fraction of roughly 10% of all A-type stars shows the peculiarities and notable magnetic fields. Ap stars typically rotate more slowly than normal A stars. The distributions do overlap, but the Ap stars form a separate distribution and are not just a slow tail of the period distribution of normal A stars (Abt & Morrell 1995).

The magnetic fields have typically strengths of a few kGauss and are not symmetric with respect to the rotation axis. The variety of field strengths and geometries is large. Measured fields are between 0.3 and 30 kG (Donati & Landstreet 2009). Especially the very slow rotators among the Ap stars do not show any strong magnetic fields of above 7.5 kG (Mathys 2008). An approximation of the magnetic fields by dipoles leads to an axis of obliquity against the rotation axis. This was shown to be large (inclined dipole) for the faster of the Ap stars and smaller (aligned dipole) for the slower rotators by Bagnulo et al. (2002). This picture was modified by Mathys (2008) who found very large obliquity values also for the extremely slowly rotating Ap stars.

There are also differing results on the evolutionary picture of magnetic intermediate-mass stars. Hubrig et al. (2000) found the Ap star phenomenon to be much less frequent among stars which have not completed the first 30% of their main-sequence life. This was challenged by Landstreet et al. (2007) who attributed at least part of the effect to the difficulties in determining the ages of these stars. Young intermediate-mass stars also show magnetic fields, and the fraction of magnetic ones of the total number is roughly the same as for Ap stars (about 7%, Wade et al. 2009), indicating that Ap star magnetism persists from the pre-main-sequence phase into the main sequence. In a study relating the magnetic field strength to the age, Hubrig et al. (2009) found a decrease of field strength with age where the stars were between 0.3 and 14 Myr old, concluding that Herbig Ae/Be stars are not the progenitors of Ap stars.

2 Ap star magnetism from Tayler instability

Nearly all magnetic-field configuration are prone to instability eventually, if the field strength is large enough. Magnetic fields $\boldsymbol{B}$ pertaining to electrical currents $\boldsymbol{j}$ will become unstable unless they are force-free, i.e. $\boldsymbol{B}||\boldsymbol{j}$ or are balanced by other forces (Duez et al. 2010). Comprehensive studies of toroidal magnetic fields were published by Vandakurov (1972) and Tayler (1973). In many cases, non-axisymmetric perturbations are the most unstable ones. The term kink-instability refers to these cases. We will refer to the whole class of current-driven instabilities by the term Tayler instability and will not review the extensive research that has been done on current-driven instabilities here.

Rotation stabilizes the magnetic fields. A rough estimate tells that magnetic fields become unstable if $\Omega_{\rm A} \sim \Omega$, where $\Omega_{\rm A} = B/\sqrt{\mu\rho}\, r \sin\theta$ is the Alfvén angular velocity and Ω is the angular velocity of the domain storing the fields (Pitts & Tayler 1985). At the expense of longer growth times,

⋆ Corresponding author: rarlt@aip.de

smaller fields can also become unstable. According to computations by Arlt et al. (2007a) and Kitchatinov & Rüdiger (2008), the magnetic fields stored in the solar tachocline would be limited to a few hundred Gauss. They can be stabilized further by adding a poloidal magnetic field, the stability limit then being about 1000 Gauss (Arlt et al. 2007b) which still corresponds to fields with $\Omega_{\rm A} \ll \Omega$.

The stability against non-axisymmetric perturbations is additionally enhanced if differential rotation is present. According to the analysis by Rüdiger & Kitchatinov (2010), a weak differential rotation of a few per cent is already enough to increase the stability limit for the $m = 1$ mode by a factor of three, where m is the azimuthal wave number. The computations were global in the horizontal direction and local in the radial direction. We will look at the global three-dimensional behaviour in the following study.

Since the magnetic fields of Ap stars are virtually constant in time, it is interesting to find stable magnetic field configurations which are not Tayler unstable and could thus provide the constant fields observed. Braithwaite & Nordlund (2006) have computed such equilibria for a non-rotating star. They are twisted tori in which the poloidal component is the main contributor to the magnetic energy. More complex structures of surface magnetic fields were found by Braithwaite (2008).

We are going another way here: the idea is that the observed surface magnetic fields of Ap stars are *not* the manifestation of initially stable magnetic-field configurations, but that they are the result of unstable magnetic fields. We explore the possibility that the observed fields are remnants of the Tayler instability of toroidal fields in the stellar interior.

3 Numerical model

The simulations employ a spherical shell to mimic the radiative envelope of an Ap star. The computational domain extends from an inner radius of $r_{\rm i} = 0.5$ to an outer radius of $r_{\rm o} = 1$ in normalized units. We need to emphasize though that the simulations are not meant to cover the very outer zones of the star which are characterized by low density and considerably different physics as compared to the bulk of the purely radiative zone. The system is simplified to the Boussinesq approximation which ignores variations of the background density ρ in space and time. It does allow for small density deviations from the background value thus permitting also simulations of convection with which we are not concerned here. The solutions are obtained with the spherical spectral MHD code by Hollerbach (2000).

The simulations are carried out in non-dimensional units, where lengths are measured in terms of the stellar radius R_*, times in diffusion times, $\tau_{\rm diff} = R_*^2/\eta$ with η being the magnetic diffusivity, and thus velocities and magnetic fields in terms of η/R_* and $\sqrt{\mu\rho}\,\eta/R_*$, respectively, where μ is the magnetic permeability. The following non-dimensional equations evolve the velocity $\boldsymbol{u}$, the magnetic field strength $\boldsymbol{B}$, and the temperature deviation Θ from a given background temperature profile T_0:

$$\frac{\partial \boldsymbol{u}}{\partial t} = -(\boldsymbol{u}\cdot\nabla)\boldsymbol{u} + (\nabla\times\boldsymbol{B})\times\boldsymbol{B} + \widetilde{\rm Ra}\,\boldsymbol{r}\,\Theta - \nabla p + {\rm Pm}\triangle\boldsymbol{u}, \quad (1)$$

$$\frac{\partial \boldsymbol{B}}{\partial t} = \nabla\times(\boldsymbol{u}\times\boldsymbol{B}) + \triangle\boldsymbol{B}, \quad (2)$$

$$\frac{\partial \Theta}{\partial t} = -\boldsymbol{u}\cdot\nabla\Theta - \boldsymbol{u}\cdot\nabla T_0 + \frac{\rm Pm}{\rm Pr}\triangle\Theta, \quad (3)$$

where p is the pressure, the Prandtl number Pr is the ratio of the viscosity ν to the thermal diffusivity χ, ${\rm Pr} = \nu/\chi$ while the magnetic Prandtl number Pm is the ratio of ν to the magnetic diffusivity η, ${\rm Pm} = \nu/\eta$. The ratio of Pm to Pr is often called the Roberts number q. The density ρ and the permeability μ are set to unity. The background temperature profile follows

$$T_0 = \frac{r_{\rm o}r_{\rm i}/r - r_{\rm i}}{r_{\rm o} - r_{\rm i}} \quad (4)$$

accounting for an entirely conductive heat transport with upper and lower boundary values of 0 and 1, respectively.

The initial velocity field is a differential rotation according to

$$\Omega(s) = \frac{\rm Rm}{\sqrt{1+s^q}}, \quad (5)$$

where $s = r\sin\theta$ is the distance from the rotation axis and Rm is the magnetic Reynolds number defined by

$${\rm Rm} = \frac{R_*^2\Omega_*}{\eta}, \quad (6)$$

where Ω_* is the angular velocity of the star. Lines of constant Ω are parallel to the rotation axis and cause the least amount of hydrodynamically induced meridional flows in which we are not interested here. We assume that the star has undergone a rotational braking before entering the main sequence (Stępień 2000). Since this braking has affected the surface of the star, a differential rotation near the ZAMS may be a good model for at leatst some of the young intermediate-mass stars. We are using ${\rm Rm} = 20\,000$, $q = 4$, and ${\rm Pm} = 1$ in all computations. There is a single simulation employing ${\rm Rm} = 40\,000$.

Magnetic fields are measured in terms of Lundquist numbers, which is the same as the non-dimensional Alfvén velocity in our system of units,

$$B = \frac{RB_{\rm phys}}{\sqrt{\mu\rho}\,\eta}. \quad (7)$$

The initial magnetic field is a poloidal field of strength $B_0 = 300$ which is entirely confined in the computational domain. This condition is not a requirement for the instability, but it ensures that the radial fields finally measured on the surface of the star are not relics of the initial-field configuration.

In time-dependent simulations, the magnetic diffusivity η is far from the stellar one and typically represents a value between the microscopic diffusivity of the plasma and the turbulent diffusivity resulting from, e.g., averaged convective motions. Of the quantities entering (7), η is the one

Table 1 The simulations described in this Paper. In the symmetry column, S means symmetric and A means antisymmetric with respect to the equator. $B_{\rm top}$ is the dimenionless maximum magnetic field at the surface, while $t_{\rm top}-t_{\rm pert}$ is the time when this maximum occurs, measured as a difference to the instance of perturbation in diffusion times.

Run	Initial symmetry	$\widetilde{\rm Ra}$	$B_{\rm top}$	$t_{\rm top}-t_{\rm pert}$
NLA0	$\boldsymbol{u}$: S, $\boldsymbol{B}$: A	0	1075	0.00296
NLS0	$\boldsymbol{u}$: A, $\boldsymbol{B}$: S	0	167	0.00494
NLA-1E9	$\boldsymbol{u}$: S, $\boldsymbol{B}$: A	$-1\cdot10^9$	199	0.00582
NLS-1E9	$\boldsymbol{u}$: A, $\boldsymbol{B}$: S	$-1\cdot10^9$	64	0.00914
NLS-5E9	$\boldsymbol{u}$: A, $\boldsymbol{B}$: S	$-5\cdot10^9$	60	0.00842

which is known least. It is therefore best to eliminate η by Rm and thus retrieve the physical magnetic fields by comparing its Alfvén speed with the rotational velocity,

$$B_{\rm phys}=\sqrt{\mu\rho}\,\Omega_* R_* \frac{B}{\rm Rm}. \quad (8)$$

The boundary conditions for the flow are stress-free at both $r_{\rm i}$ and $r_{\rm o}$. There is no imposed velocity, neither in the bulk of the computational domain nor at the boundaries. Vacuum conditions are employed at both $r_{\rm i}$ and $r_{\rm o}$ for the magnetic field. Such conditions may look odd at the inner boundary, but it is a fairly good way of getting the least amount of artifacts from the inner boundary which, as such, does not exist in reality. Perfect-conductor conditions are much worse, since they cause strong currents near the inner boundary as soon as the magnetic field tends to fill the whole stellar interior from $r=0$ to $r_{\rm o}$ which is prevented by the boundary conditions.

Note that the use of spherical harmonics allows the implementation of exact vacuum conditions which are not straight-forward in grid codes. The boundary conditions for the temperature fluctuations are $\Theta(r_{\rm i})=0$ and $\Theta(r_{\rm o})=0$.

The velocity and the magnetic field are expressed by two scalar potentials each. These and the temperature fluctuations are decomposed in Chebyshev polynomials in the radial direction and in spherical harmonics for the horizontal directions. The potentials are thus functions of the Chebyshev degree k, the Legendre degree l, the azimuthal wave number m, and the time t. The spectral truncations were at $k_{\rm max}=40$ Chebyshev polynomials and all spherical harmonics up to $l_{\rm max}=60$ and m running from $-l$ to l.

An implicit scheme integrates the diffusive terms in spectral decomposition, whereas the nonlinear terms are treated on a collocation grid in real space. We implemented a variable time-step determined by the Courant-Friedrich-Levy (CFL) criterion from the velocity and the Alfvén velocity of the magnetic field. An additional safety factor of 0.2 is applied to the maximum possible time-step according to the CFL criterion. Since a new time-step requires expensive inversions of the time-stepping matrices for all five variables, we update the time-step only every 100 integration steps. This is certainly a compromise but turned out to ensure – together with the safety factor of 0.2 – enough stability to run the code through the injection and growth of the unstable mode.

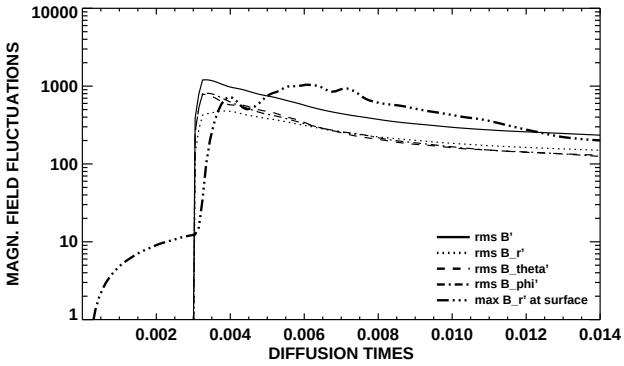

Fig. 1 Magnetic field fluctuations as functions of time for the run NLA0 with $\widetilde{\rm Ra}=0$ and a perturbation which is antisymmetric in $\boldsymbol{B}$.

4 Results

All the simulations are first evolving the axisymmetric initial conditions in a three-dimensional domain. The energy in the non-axisymmetric modes remains about 30 orders of magnitude smaller than the energy in the $m=0$ mode. The differential rotation winds up the initial poloidal magnetic field very quickly. At the same time, Maxwell stresses grow and diminish the differential rotation. The whole process reaches a maximum toroidal field after a time which can be estimated by $t_{\rm grow}=\sqrt{\mu\rho}R_*/B_0$. In our case with $B_0=300$, this corresponds to a dampig time for the differential rotation of $t_{\rm damp}=0.0033$ diffusion times. Note that this time-scale does not depend on the Reynolds number. In a system of coupled equations of motion and induction, a stronger differential rotation also means stronger magnetic fields and thus stronger Maxwell stresses changing the differential rotation.

An earlier stability analysis delivered the maximum field strength of the axisymmetric configuration, beyond which the system becomes unstable under non-axisymmetric perturbations (Arlt & Rüdiger 2010). In the present study, we inject a non-axisymmetric perturbation into the system at $t_{\rm pert}=0.003$ diffusion times which is when the axisymmetric configuration is already supercritical. The perturbation has the topology of a $P_2^1(\cos\theta)\cos\phi$ spherical harmonic for the antisymmetric cases ('A' in Table 1) and that of a $P_2^1(\cos\theta)\cos\phi$ spherical harmonic for the symmetric cases ('S' in Table 1) in the poloidal potential of the magnetic field. This also corresponds to an antisymmetric and a symmetric magnetic field perturbation, respectively. The simulations presented here are listed in Table 1.

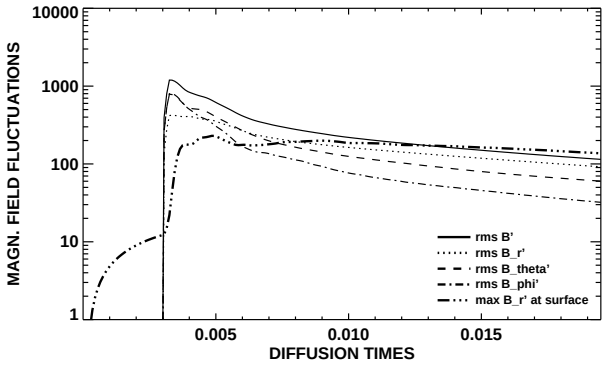

Fig. 2 Magnetic field fluctuations as functions of time for the run NLA-1E9 with $\widetilde{\mathrm{Ra}} = -10^9$ and a perturbation which is antisymmetric in $\boldsymbol{B}$.

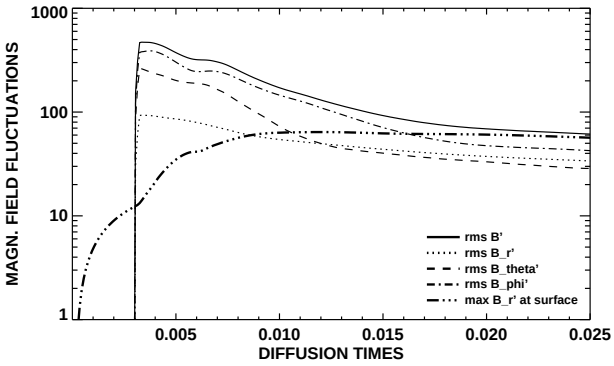

Fig. 4 Magnetic field fluctuations as functions of time for the run NLS-1E9 with $\widetilde{\mathrm{Ra}} = -10^9$ and a perturbation which is symmetric in $\boldsymbol{B}$.

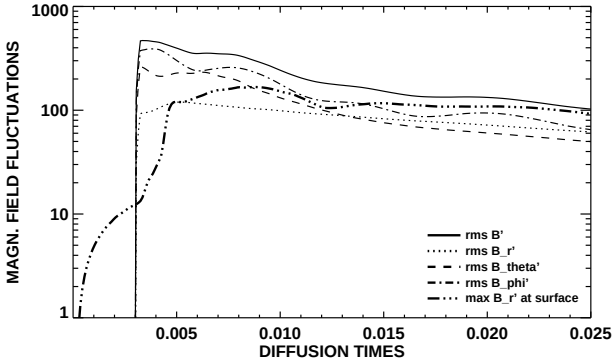

Fig. 3 Magnetic field fluctuations as functions of time for the run NLS0 with $\widetilde{\mathrm{Ra}} = 0$ and a perturbation which is symmetric in $\boldsymbol{B}$.

The nonlinear evolution of the instability of a perturbation which is antisymmetric in the magnetic field (run NLA0; resulting in a symmetric flow perturbation) is shown in Fig. 1 for $\widetilde{\mathrm{Ra}} = 0$ in terms of the rms magnetic field components $B_r^{\mathrm{rms}} = \sqrt{\langle B_r'^2 \rangle}$ etc. The maximum radial magnetic field B_r^{max}, determined only on the outermost surface of the collocation grid, is also shown. The surface is located at a distance of $\Delta r = 5 \cdot 10^{-5}$ from the outer radial boundary. It is interesting to note that the maximum surface radial field supercedes the rms values of the internal fluctuating magnetic field. The corresponding run NLA-1E9 with $\widetilde{\mathrm{Ra}} = -10^9$ is shown in Fig. 2. The emerging fields are lower in general, and the maximum is reached at a later time. The maximum B_r at the surface remains almost constant for the rest of the simulation.

Figures 5 and 6 show the surface magnetic fields of the simulations NLA0 and NLA-1E9, respectively. Both are taken at the moment when the radial surface field reaches its maximum; these are at $t - t_{\mathrm{pert}} = 0.00296$ diffusion times for NLA0 and at $t - t_{\mathrm{pert}} = 0.00582$ for NLA-1E9. The $m = 1$ mode is evidently the dominating one for NLA-1E9, while the run with $\widetilde{\mathrm{Ra}} = 0$ shows much smaller azimuthal scales. Stable stratification seems to cause smoother surface fields in general, regardless of the symmetry of the perturbation, and also weaker magnetic fields. A purely antisymmetric solution has to show $B_r = 0$ in the equatorial plane of the rotating sphere, thereby excluding an obliquity of $90°$. It is thus interesting to excite a symmetric mode by a symmetric perturbation, and to test whether maximum obliquity can be achieved.

Figures 3 and 4 show the corresponding rms magnetic fields for symmetric perturbations. The fields emerging are typically weaker and tend to reach their maximum about 20–30% later than the fields emerging from an antisymmetric perturbation. Both symmetries have been shown to be unstable in the analysis by Arlt & Rüdiger (2010) near $t = 0.003$. However, a look at the surface plots in Figs. 7 and 8 tells us that there is no pure symmetry anymore after a certain time; the plots were made at the times of maximum surface field, i.e. $t - t_{\mathrm{pert}} = 0.00494$ diffusion times for NLS0 and at $t - t_{\mathrm{pert}} = 0.00914$ diffusion times for NLS-1E9, respectively. Numerical noise is apparently growing and delivering a substantial contribution from the antisymmetric mode. We conclude that antisymmetric configurations are more likely to become visible on the stellar surface than symmetric ones. This of course excludes an obliquity of precisely $90°$.

The field strengths appearing at the surface are quite substantial. They range from 4% to 76% of the maximum toroidal field strength inside the computational domain. The corresponding field strengths are between 1 kG and 29 kG according to (8) for stars with radii between $1.5 R_\odot$ and $2.5 R_\odot$ and a rotation period of 10 days. This is a nice match with the observed surface magnetic fields. For longer rotation periods, the dimensionless field strengths correspond to smaller physical field strengths.

The next question concerns the time it takes a real star to show substantial fields on their surfaces, as a result of the Tayler instability of internal toroidal fields. Questions

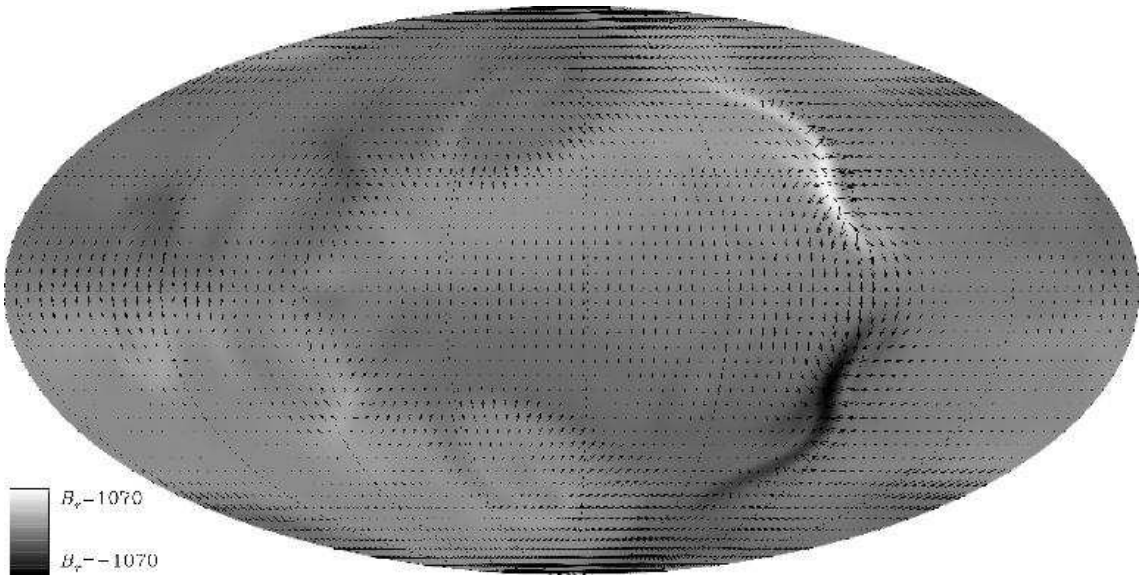

Fig. 5 Surface plot of the magnetic field from the simulation NLA0 at $t - t_{\rm pert} = 0.00296$. The contours represent B_r while the arrows show B_θ and B_ϕ. For the sake of clarity, a smaller number of arrows is plotted as compared to the actual number of collocation points in the simulation.

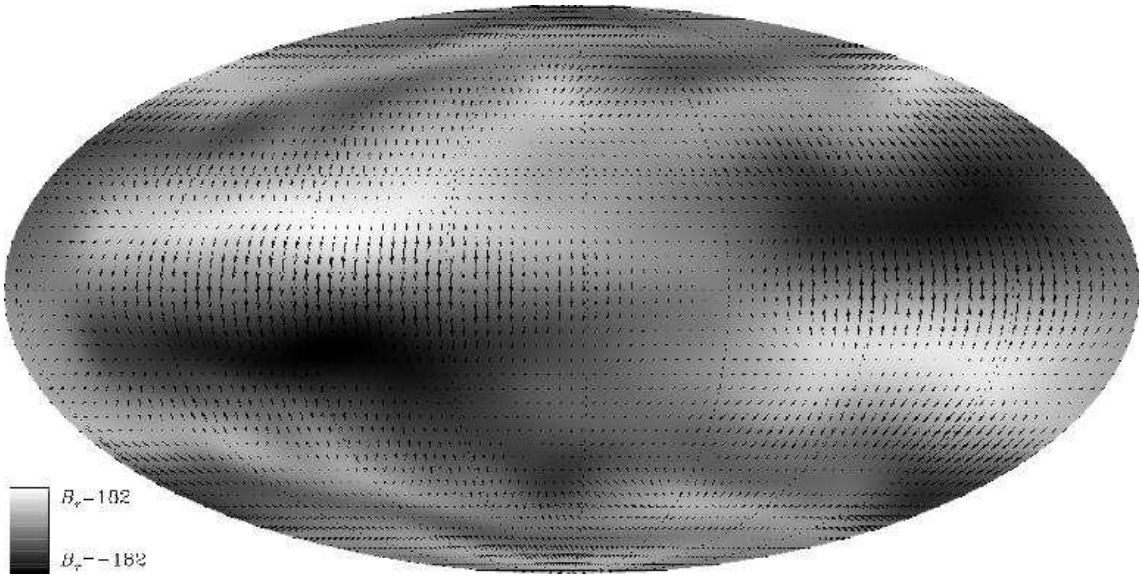

Fig. 6 Surface plot of the magnetic field of the simulation NLA-1E9 at $t - t_{\rm pert} = 0.00582$. The contours represent B_r while the arrows show B_θ and B_ϕ.

about time-scales are always difficult to answer from nonlinear simulations since the magnetic Reynolds number will always be much smaller than the stellar one. This either means that the angular velocity in the simulation is way too small, or the magnetic diffusivity is much larger than the microscopic value in stars. It is thus necessary to run simulations at various magnetic Reynolds numbers to see how the results scale with Rm.

While a full exploration of this dependence goes beyond the scope of this paper, we ran a simulation like NLS0, but with $\mathrm{Rm} = 40,000$ and obtain a time of maximum surface field of $t_{\rm top} - t_{\rm pert} = 0.00242$. The results indicate a $t_{\rm top} - t_{\rm pert} \sim \mathrm{Rm}^{-1}$ dependence. That has the advantage that the emergence time is simply a multiple of the angular velocity Ω:

$$t_{\rm phys} = \frac{C}{\mathrm{Rm}} \frac{R_*^2}{\eta} = \frac{C}{\Omega}, \tag{9}$$

where $C = 98$ is the result of fitting the two points with a power law. A 10-day rotation period of the star results in an emergence after 0.43 yr for NLS0, while it is ten times longer for a 100-day rotation period. The longest emergence

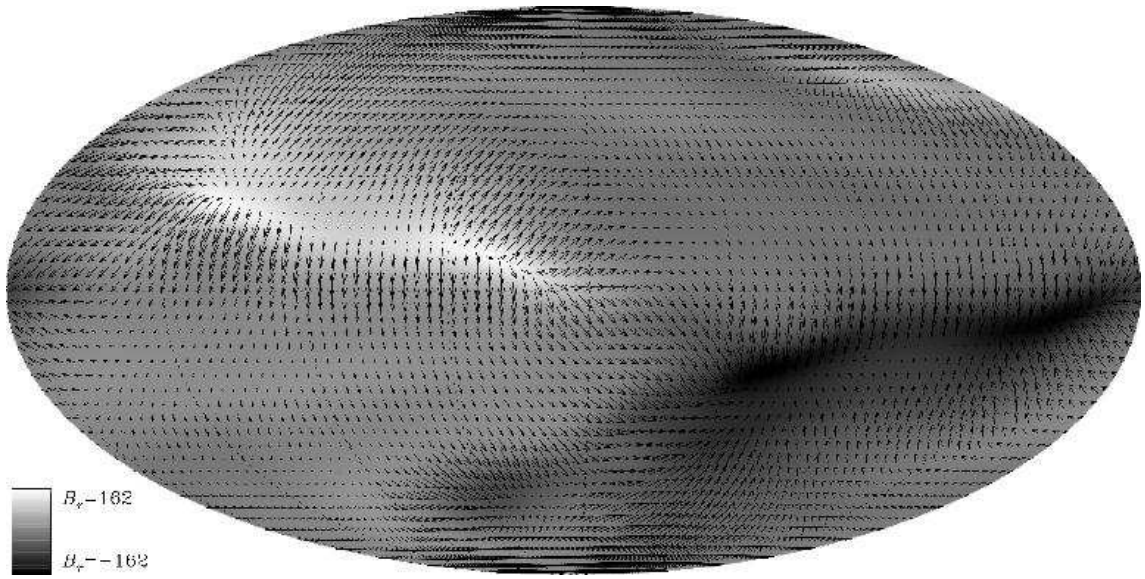

Fig. 7 Surface plot of the magnetic field from the simulation NLS0 at $t - t_{\rm pert} = 0.00494$. The contours represent B_r while the arrows show B_θ and B_ϕ.

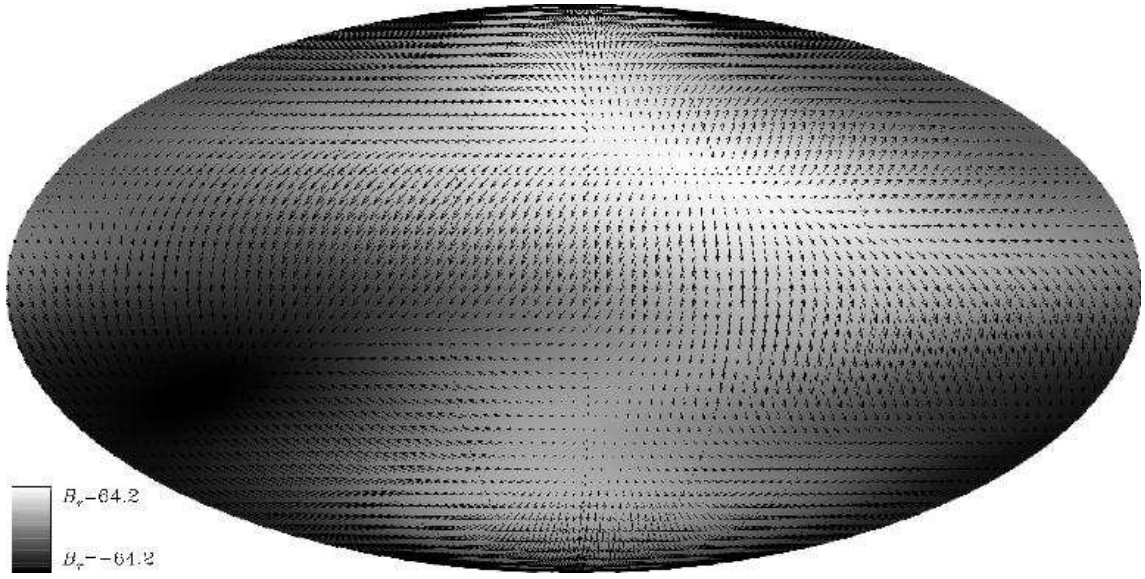

Fig. 8 Surface plot of the magnetic field from the simulation NLS-1E9 at $t - t_{\rm pert} = 0.00914$. The contours represent B_r while the arrows show B_θ and B_ϕ.

delays seen in the simulations are about 8 yr with a strongly stable stratification.

5 Discussion

We simulated the nonlinear, three-dimensional evolution of the Tayler instability in a spherical shell. The instability provides magnetic field configurations of mostly large scales with a preference to modes which are nonaxisymmetric and antisymmetric with respect to the equator. The field strength of the maximum radial magnetic field at the stellar surface was found to be between 1 and 29 kG which is what is observed on most Ap stars. The emergence of the remnant fields from the instability at the surface of the star is delayed by several tens of stellar rotations. This estimate holds only if $t_{\rm top} - t_{\rm pert} \sim \Omega^{-1}$, however. In reality, it is a lower limit for the emergence delays.

This is certainly a too simple way of getting the time delays between the instability and flux emergence at the surface, but we can conclude that the time necessary to observe the remnant fields are shorter than evolutionary time-scales. By contrast, Arlt & Rüdiger (2010) argued that the flux rise is of diffusive nature and obtained delays of several Myr. The present study indicates that the time-scale

will be shorter. As a consequence, if magnetic fields would appear on Ap stars at later times during their evolution, it must be by other factors which influence the stability limits of the potentially stored toroidal fields. Since the instability as well as the rise of fields to the surface are very fast, it is highly unlikely that the phenomenon itself is seen in progress.

As the instability drains energy from the magnetic field, the growth quickly halts and the remaining magnetic field suffers only from the flows excited by the instability and from Ohmic diffusion which is very slow. The rms velocities are about three times weaker than the rms magnetic fields shown in Figs. 1–4 and do not cause quick changes of the surface structure. This gives the impression of stationary magnetic fields, while the period of instability is very short and most likely missed by observations.

The finding by Mathys (2008) that the very slow rotators are not hosting any fields above 7.5 kG would be compatible with the fact that an originally slower rotation of the pre-main-sequence star has not allowed very strong toroidal fields to build up, since the instability limit is lower for slow rotation, whence the smaller remnant fields from the Tayler instability.

The drawback of the present approach is the Boussinesq approximation which is actually valid for small deviations from the adiabatic temperature gradient. The imitation of a very stable stratification by a highly negative $\widetilde{\mathrm{Ra}}$ is still telling us qualitative features of the emergence of surface fields, but quantitatively, we need to be careful with emergence times and flux. The same also holds for computations in the anelastic approximation. First computations of the scenario in a fully compressible spherical shell are on the way.

Normal A stars would thus still be hosting considerable toroidal fields. The emergence times of stable magnetic-field configurations are very long and probably beyond 100 Myr (Mestel & Moss 2010). Since they rotate typically faster than Ap stars, normal A stars may have a higher threshold for the Tayler instability and could thus be able to keep strong toroidal magnetic fields in their interiors without showing substantial fields on the surface. The implication would be, however, that as soon as the stars start to become giants, their radii grow, and the rotation periods increase substantially. The fields will no longer be stabilized and must become unstable. This would imply that nearly all stars on the giant branch having intermediate-mass stars as progenitors should show magnetic fields. These are of course much weaker because of the larger radius and the steep decrease of field strength with radius, especially for higher modes than dipoles. The giant EK Eri has been considered a descendant of an Ap star (Stępień 1993; Dall et al. 2010), i.e. the star would have shown surface magnetic fields through nearly all its life. However, the magnetic fields may have been emerging only when the star evolved away from the main sequence and became a slow rotator, and the progenitor would actually be a normal A star. Since the star has a relatively low mass among the "A-star descendants" its age of roughly 1 Gyr may be even compatible with the diffusive emergence of fields discussed by Mestel & Moss (2010) though.

The critical question now is how Ap stars are discriminated from normal A stars in an early stage of stellar evolution. This problem cannot be solved in the context of this Paper, but it is suggested that it is differences in the rotational evolution during the pre-main-sequence phase that decides whether stars evolve into normal A stars or Ap stars. It would not be necessary to think of a presence or absence of magnetic fields during star formation. These "primordial" fields are most likely processed during the Hayashi phase and will be highly modified.

References

Abt, H.A., Morrell, N.I.: 1995, ApJS 99, 135
Arlt, R., Rüdiger, G.: 2010, MNRAS, in press
Arlt, R., Sule, A., Rüdiger, G.: 2007a, A&A 461, 295
Arlt, R., Sule, A., Filter, R.: 2007b, A&A 328, 1142
Bagnulo, S., Landi Degl'Innocenti, M., Landolfi, M., Mathys, G.: 2002, A&A 394, 1023
Braithwaite, J.: 2008, MNRAS 386, 19447
Braithwaite, J., Nordlund, Å.: 2006, A&A 450, 1077
Dall, T.H., Bruntt, H., Stello, D., Strassmeier, K.G.: 2010, A&A 514, A25
Donati, J.-F., Landstreet, J.D.: 2009, ARA&A 47, 333
Duez, V., Braithwaite, J., Mathis, S.: 2010, ApJ 724, 34
Hollerbach, R.: 2000, Int. J. Num. Meth. Fluids 32, 773
Hubrig, S., North, P., Mathys, G.: 2000, ApJ 539, 352
Hubrig, S., Stelzer, B., Schöller, M., et al.: 2009, A&A 502, 283
Kitchatinov, L.L., Rüdiger, G.: 2008, A&A 478, 1
Mathys, G.: 2008, Contrib. Astron. Obs. Skalnaté Pleso 38, 217
Landstreet, J.D., Bagnulo, S., Andretta, V., Fossati, L., Mason, E., Silaj, J., Wade, G.A.: 2007, A&A 470, 685
Mestel, L., Moss, D.: 2010, MNRAS 405, 1845
Pitts, E., Tayler, R.J.: 1985, MNRAS 216, 139
Rüdiger, G., Kitchatinov, L.L.: 2010, Geophys. Astrophys. Fluid Dyn. 104, 273
Stępień, K.: 1993, ApJ 416, 368
Stępień, K.: 2000, A&A 353, 227
Tayler, R.J.: 1973, MNRAS 161, 365
Vandakurov, Yu.V.: 1972, SvA 16, 265
Wade, G.A., Alecian, E., Grunhut, J., Catala, C., Bagnulo, S., Folsom, C.P., Landstreet, J.D.: 2009, astro-ph/0901.0347